03,09

Investigation of electrical resistance and thermal EMF of a single crystal of samarium monosulfide under temperature cycling in the range 320−800 K

© N.N. Stepanov, G.A. Kamenskaya, S.V. Novikov

Ioffe Institute,
St. Petersburg, Russia

E-mail: stnick@mail.ioffe.ru

Received October 23, 2023
Revised October 23, 2023
Accepted October 24, 2023

The study of the temperature dependences of the electrical resistance R and thermal EMF S of a single crystal of samarium monosulfide SmS in two cycles in the range 320−800 K. It has been established that cyclic temperature action has a significant effect on the processes of electrical transfer in the test sample, which is found in hysteresis phenomena on the dependences of $\ln[R(10^3/T)]$ and $S(T)$, as well as in changes in the behavior of the latter in the high-temperature region, both due to rearrangement of the impurity and exciton spectra, and the participation of in electronic transport the 5*d*-subzone of the SmS conduction band.

Keywords: samarium monosulfide, thermal EMF, temperature cycling, electrical resistance.

DOI: 10.61011/PSS.2024.01.57848.237

1. Introduction

Samarium monosulphide (SmS) is one of the most extensively studied compounds over the previous decades — representatives of rare earth element (REE) semiconductor monochalcogenide family. The given material has a set of unique physical and chemical properties, including, in particular, structural and electronic phase transformations in a broad thermobaric region, and a record-breaking piezoresistive effect [1–4]. At the same time, the electronic spectrum structure and evolution of SmS under the effect of changing external thermodynamic parameters that cause the rearrangement of its crystal lattice and electrotransport properties variation have not been finally understood yet.

This paper describes the findings of the experimental study of behavior of resistance R and thermal emf S of samarium monosulphide single-crystal in the temperature range of 320−800 K. Such investigations were necessitated by the fact that the previous high-temperature measurements of R and S [1,5] conducted in different time on SmS single-crystals produced in a single process cycle differ considerably. This, in particular, is applicable to behavior $S(T)$ of SmS single-crystal samples in [1] and [5] in the covered temperature range,and to temperature dependences $\ln R(10^3/T)$ that differ in positions of the function curve knee points on the x axis of the reciprocal temperature scale (with weight coefficient 10^3).

Considering the aforesaid, the objective of the study was to verify the previous data on temperature dependences $R(T)$ and $S(T)$ of samarium monosulphide single-crystals by conducting repetitive experiments on a SmS single-crystal separately synthesized using a proven procedure (see the link below).

The review of the experimental data obtained herein, a set of assumptions is made as to the features of the electronic spectrum structure and transport properties of charge carriers in SmS in the range of 320−800 K.

2. Experimental procedure

Stoichiometric SmS single-crystals were prepared using technique [6]. $\sim 12 \times 5 \times 2$ mm test sample was chipped out from a synthesized ingot on material cleavage plane [100].

According to the X-ray diffraction analysis, the crystal lattice constant of the test sample at $T = 300$ K and atmospheric pressure $P = 0.1$ MPa was equal to $a_{\mathrm{SmS}} = 5.968$ Å (SG $Fm\bar{3}m$); the X-ray coherent scattering region (CSR) was $L_{\mathrm{SmS}} \sim 2500$ Å, which corresponds to a quite well-formed single-crystal. The parameters listed above are fully identical to those published earlier in [7], including also the presence of a low amount, lower than 1%, of impurities (mainly samarium oxysulphide Sm_2O_2S) that do not have any considerable influence on the electrotransport in SmS due to their low conductivity.

Resistivity and thermal emf of SmS at $T = 300$ K and atmospheric pressure were, respectively, equal to $\rho \sim 11\,\mathrm{m\Omega \cdot cm}$ and $S \sim -280\,\mu\mathrm{V/K}$; the test sample demonstrated the semiconductor conductivity behavior ($\partial\rho/\partial T < 0$). In the specified temperature and pressure conditions, electrotransport in SmS is adequately described within the band spectrum model [8].

Temperature dependences of resistivity R and thermo emf S of SmS single-crystals in the region from 320 to 800 K were examined on the system described in detail in [9].

Two measurement cycles of R and S were conducted in temperature cycling conditions („heating-cooling“).

Temperature trend of the resistivity R of SmS single-crystal was studied by the four-probe AC method using spring-loaded platinum contacts. Similarly, two Pt-Pt/Rh thermocouples were used to measure the temperature and temperature gradient along the maximum dimension of the sample; thermal emf S recorded during the experiment were calculated considering the thermal emf Pt (the measurement procedure is described in [9]).

3. Measurement data

Figure 1 shows the dependences of log resistance R of SmS single-crystal on the reciprocal temperature with weight coefficient 10^3 for two thermal measurement cycles (thermal cycles). It should be noted that upon completion of the first thermal cycle, the test sample resistance increased by 4.5%. As a result of repeated thermal cycle, growth of R SmS did not exceed 3%.

Figure 2 shows thermal emf-temperature dependences of SmS for two thermal cycles. The Figure shows that sample heating and cooling curves S in the first thermal cycle differ significantly from each other at low temperatures. With it, the absolute value of thermal emf of the sample increases considerably. In the second thermal cycle, curves S are not much different from each other in heating and cooling, however, thermal emf in heating is a little higher than that in cooling. Let's consider the possible causes of R and S variations in SmS as a result of conducted experiments.

4. Analysis of findings

Cyclic high-temperature exposure of the SmS sample has a significant effect on the crystal lattice defect structure with simultaneous rearrangement of the donor and acceptor state spectrum in the given compound [10]. In turn, energy state spectrum variations in the SmS band gap affect the temperature dependences of the transport coefficients. Thus, Figure 1 shows the growth of resistance R with respect to initial value upon completion of the measurement procedure in the first thermal cycle. The identified fact may be caused by several causes. First, heating of the sample in vacuum at high temperatures causes evaporation of sulfur atoms from the surface and, thus, a diffusion flux from the sample volume occurs to compensate the loss of anions. Second, the sulfur vacancies formed within the sample are filled with samarium cations that were previously located in the crystal lattice interstices. Possibility of such process was justified in [10]. Since the transition of samarium cations from interstices to vacant positions in the sulfur sublattice is energetically favorable, the ionization potential of $4f$-electrons of Sm^{2+} transferred to the anion positions in the regular crystal lattice grows. The latter results in a decrease in current carrier concentration in the conduction band and, therefore, in resistivity growth

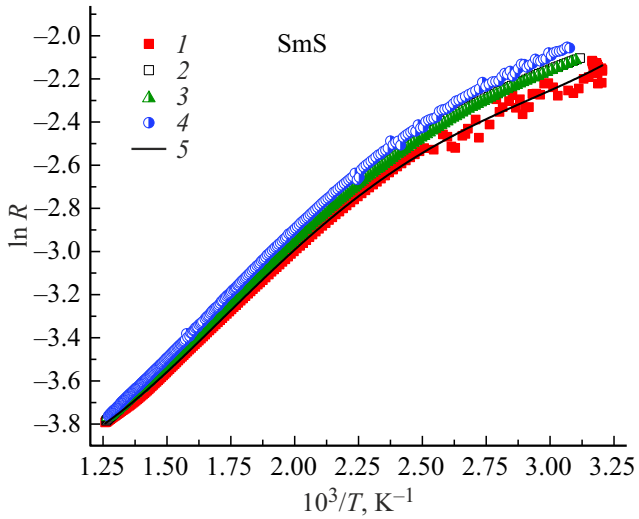

Figure 1. Temperature dependences $\ln R$ of SmS single-crystal on reciprocal temperature with weight coefficient 10^3 for two measurement cycles *1* — heating, cycle 1, *2* — cooling, cycle 1, *3* — heating, cycle 2, *4* — cooling, cycle 2, *5* — polynomial approximation line.

of the SmS sample in the initial temperature conditions. Diffusion into light nonmetal material (oxygen, nitrogen, carbon) from the residual thermostat atmosphere also takes place, whilst the light nonmetals form chemical bonds with cations and block their capability to activate electrons into the conduction band [7]. In the next thermal cycle, the situation repeats in general the only difference being in that the anion sublattice likely still contains free vacancies and vacancies filled with the aforesaid light nonmetal (O, N, C) that are responsible for partial compensation of conductivity electrons. The arguments for this assumption (additionally to [7,10]) will be provided below in the review of the experimental data of $S(T)$. It should be noted that in case of lower concentration of interstitial cations in the sample, charge and mass transport in the sample during heating in vacuum will occur mainly in the anion subsystem.

Let's review dependences $\ln[R(10^3/T)]$of SmS again. Review of the relevant curves (Figure 1) shows that they contain anomalies in the form of knees at various temperatures. To understand the factors behind the singularities found on curves $\ln[R(10^3/T)]$, we shall differentiate the specified functions by the reciprocal temperature with weight coefficient 10^3 in the function identification regions and shall build temperature dependences of derivatives $\partial R/[R\partial(10^3/T)]$ that coincide with that of the local activation energy $E_a(T)$ of free current carriers in SmS with accuracy to the constant coefficient $k_B \cdot 10^3$ (k_B — the Boltzmann constant).

Dependences $E_a(T)$ SmS calculated using the experimental data obtained in the first thermal cycle are shown in Figure 3. Review of the set of $E_a(T)$ data generally confirms the electrotransport model in SmS in the temperature range of 320−500 K through activation of electrons from donor

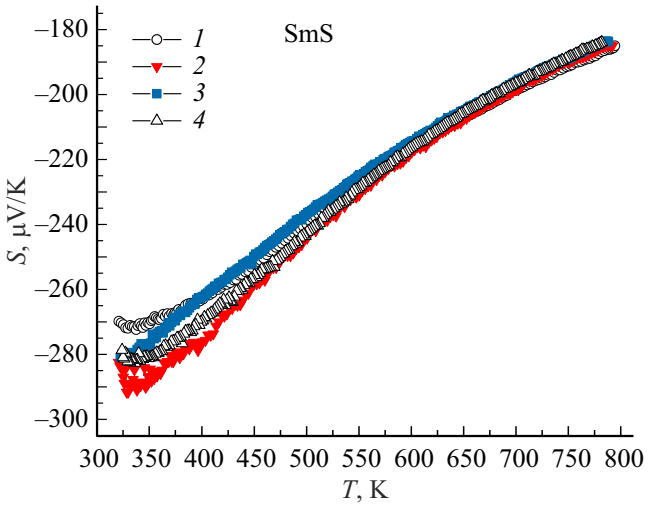

Figure 2. Thermal emf-temperature dependences of SmS for two thermal cycles *1* — heating, cycle 1, *2* — cooling, cycle 1, *3* — heating, cycle 2, *4* — cooling, cycle 2.

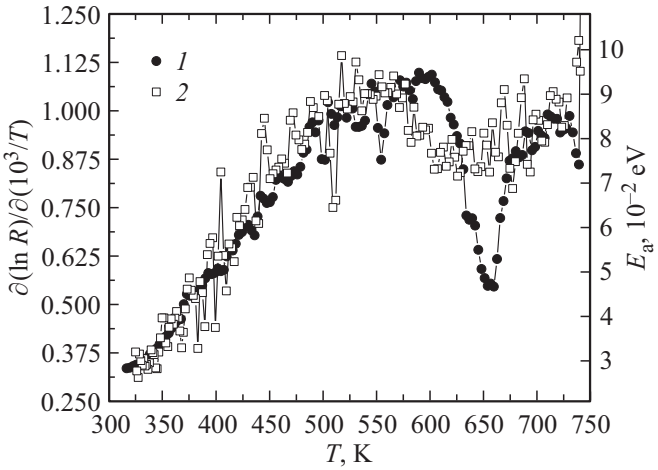

Figure 3. Temperature dependence of the local activation energy of free current carriers in SmS. *1* — heating, *2* — cooling.

levels with a depth of 0.03 – 0.06 eV with respect to the bottom of conduction band [8], or according to the earlier data [1] — 0.04–0.07 eV.

In the range of 500–550 K, SmS has some stabilization of E_a at $\sim$ 0.08 eV (Figure 3). It should be noted that in the range of 490–500 K, endothermal effect has been detected earlier in samarium monosulphide [11]. The set of facts mentioned above together with the theoretical developments of the exciton model of phase transition in SmS [12] suggests that exciton states are formed in the band gap due to $4f5d$-Coulomb interaction of electrons and vacancies.

With sample temperature rise above 550 K, exciton disintegration process develops in its electron subsystem, together with formation of excitons, which is followed by electron transition to the conduction band formed by 6*s*- and 5*d*-wave functions of Sm [2]. At temperatures exceeding 600 K, the exciton system disintegration process becomes avalanche-type, which is apparent from the failure of the local activation energy of current carriers in the narrow temperature range $600 < T < 650$ K. The following increase in the sample temperature (up to 750 K) results in gradual increase of E_a.

Hysteresis observed in the thermal cycle on $E_a(T)$ (Figure 3) is explained by the fact that an exciton state spectrum cannot be formed in the inherent instability temperature region and for its restoration the sample temperature shall decrease to the acceptable level.

Let's review the temperature dependences of the thermal emf of SmS (Figure 2). During sample heating, growth of the thermal emf is observed in the first thermal cycle and is enhanced up to the knee of $S(T)$ near $\approx$ 575 K. The given value was derived from the curve of derivative $\partial S(T)/\partial T$ shown in Figure 4. The review of data in Figure 2, 4 shows that uniform slowdown of thermal emf growth in SmS is observed in the range of 680–800 K. The experimental data suggests that such behavior of $S(T)$ in the specified temperature range is caused by the initiated rapid filling with charge carriers of the „heavy" 5*d*-subband of the SmS conduction band that is located slightly higher than the „light" 6*s*-subband [13]. During cooling of the sample, the thermal emf variation rate decreases dramatically within $580 \leq T \leq 700$ K because the exciton levels cannot be formed due to the cause described above.

Sample cooling below 580 K opens the opportunity for exciton spectrum restoration, however, further decrease in temperature results in gradual decay of exciton states and transition of electrons to ground $4f$-state, at the same time electrons from the conduction band also go to localized states. It is believed that, in the temperature region near 420 K, transition takes place from filling of localized states with activation energy $E_a \approx 0.055$ eV to those with $E_a \approx 0.045$ eV.

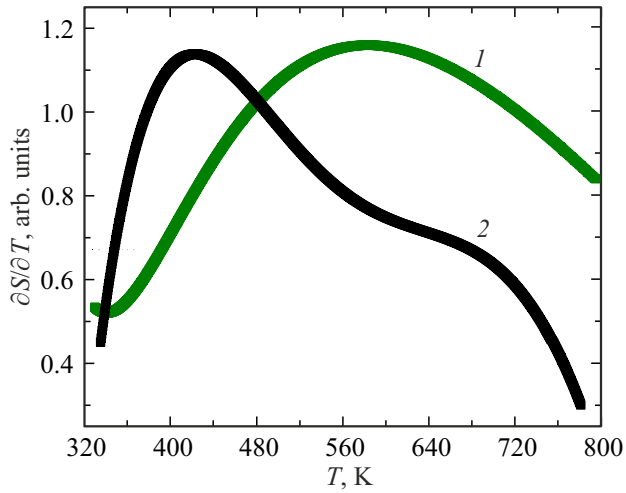

Figure 4. Temperature dependence of the thermal emf derivative $\partial S/\partial T$ of the SmS sample in the first measurement cycle (polynomial approximations). *1* — heating, *2* — cooling.

In the second measurement thermal cycle, behavior of $R(T)$ and $S(T)$ is almost unchanged, however, the hysteresis amplitudes of the specified kinetic coefficients became a little lower, which implies that, first, there is some concentration of acceptor levels in the band gap that reduce the absolute values of thermal emf of SmS and, second, there is gradual stabilization of charge carrier spectrum.

5. Conclusion

As a result of investigations of the temperature dependences of kinetic coefficients R and S in the SmS single-crystal, two temperature measurement cycles in the range of 320−800 K show significant effect of cyclic temperature exposure on the electrotransport parameters. Interpretation of the findings uses a qualitative model of the spectra rearrangement of impurity and exciton states in SmS under temperature exposure, and the known two-level layout of the conduction band of the given compound.

Conflict of interest

The authors declare that they have no conflict of interest.

References

[1] A.V. Golubkov, E.V. Goncharova, V.P. Zhuze, G.M. Loginov, V.M. Sergeeva, I.A. Smirnov. Fizicheskie svoistva khal'kogenidov redkozemel'nykh elementov. Nauka, L. (1973). 304 s. (in Russian).
[2] I.A. Smirnov, V.S. Oskotsky. UFN **124**, *2*, 241 (1978). (in Russian).
[3] T. Le Bihan, S. Darracq, S. Heathman, U. Benedict, K. Mattenberger, O. Vogt. J. Alloys Compd. **226**, *1−2*, 143 (1995).
[4] V.V. Kaminsky, M.V. Romanova. Pribory i sistemy upravleniya **8**, 28 (1988). (in Russian).
[5] M.M. Kazanin, V.V. Kaminsky, S.M. Solovyev. ZhTF **70**, *5*, 136 (2000). (in Russian).
[6] A.V. Golubkov, V.M. Sergeeva. V sb.: Fizika i khimiya redkozemelnykh poluprovodnikov (Khimiya itekhnologiya) / Otv. red.: A.A. Samokhvalov, G.P. Skornyakov. ANSSSR UNTs, Sverdlovsk. (1977). S. 28 (in Russian).
[7] L.N. Vasilyev, V.V. Kaminsky, M.V. Romanova, N.V. Sharenkova, A.. Golubkov. FTT **48**, *10*, 1777 (2006). (in Russian).
[8] A.V. Golubkov, E.V. Goncharova, V.A. Kapustin, M.V. Romanova, I.A. Smirnov. FTT **22**, *12*, 3561 (1980). (in Russian).
[9] A.T. Burkov, A.I. Fedotov, A.A. Kas'yanov, R.I. Panteleev, T. Nakama. Nauch.-tekhn. vestn. informatsionnykh tekhnologij, mekhaniki i optiki, **15**, *2*, 173 (2015). (in Russian).
[10] V.V. Kaminsky, A.V. Golubkov, L.N. Vasiliev. FTT **44**, *8*, 1501 (2002). (in Russian).
[11] V.M. Egorov, V.V. Kaminsky. FTT **51**, *8*, 1521 (2009). (in Russian).
[12] K.A. Kikoin. ZhETF **85**, *3*, 1000 (1983). (in Russian).
[13] E.V. Shadrichev, L.S. Parfenieva, V.I. Tamarchenko, O.S. Gryaznov, V.M. Sergeeva, I.A. Smirnov. FTT **18**, *8*, 2380 (1978). (in Russian).

Translated by E.Ilinskaya